Solvent Dynamical Effects on Electron Transfer in U-Shaped Donor-Bridge-Acceptor Molecules

Subhasis Chakrabarti,[†] Min Liu,[†] David H. Waldeck,*[,†] Anna M. Oliver,[‡] and Michael N. Paddon-Row*[,‡]

Chemistry Department, University of Pittsburgh, Pittsburgh, Pennsylvania 15260, USA, and School of Chemistry, University of New South Wales, Sydney NSW 2052 Australia

Received: August 18, 2008; Revised Manuscript Received: November 26, 2008

This study explores how the electron transfer in a class of donor-bridge-acceptor (DBA) supermolecules is affected by the dynamical response of the solvent. These DBA molecules have a pendant group juxtaposed between the donor and acceptor groups (Figure 1). The pendant provides intermediate electronic coupling strengths of a few hundred wavenumbers by way of its nonbonded contacts with the donor and acceptor and it can be tuned by substituents added to the pendant. This design allows the measurement of electron transfer rates from a regime in which the mechanism is nonadiabatic to a regime in which the solvent friction modifies the rate substantially. The rate constants and mechanistic parameters are compared with the expectations of models for solvent dynamical effects on the reaction rate.

I. Introduction

The influence of solvent dynamics on chemical reactions is important for understanding chemical processes in polar and viscous solvents.[1−3] In particular, this work addresses electron transfer reactions of donor-bridge-acceptor (DBA) molecules in the solvent-controlled regime. Previous work[4,5] showed that the photoinduced electron transfer reaction for molecule **3** (Figure 1) changes from a nonadiabatic electron tunneling mechanism at high temperature in the solvent *N*-metylacetamide (NMA) to a solvent-controlled mechanism at low temperature, involving the nuclear motion as the rate-limiting step of the reaction. This mechanism change was observed in solvents having high viscosity and long Debye relaxation times but not in low viscosity solvents having short Debye relaxation times. It was postulated that the mechanism change arises from a solvent friction effect, in which the polarization relaxation time of the solvent controls the rate by controlling the characteristic time spent in the transition-state (curve-crossing) region.

The U-shaped molecules **1**, **2**, and **3** are designed so that electron transfer occurs by way of electron tunneling through the pendant group. The DBA molecules in Figure 1 have the same 1,4-diphenyl-5,8-dimethoxynaphthalene (DPMN) donor unit and 1,1-dicyanovinyl (DCV) acceptor unit connected through a highly curved bridge unit that holds the donor and the acceptor moieties at a well defined distance and fixed orientation. A pendant group is covalently attached to the bridge unit and occupies the cavity between the donor and acceptor. It has been shown that in such systems the electron tunnels from the donor to the acceptor via the pendant groups.[6−8] The semiclassical equation with a single effective quantum mode can be successfully applied to describe the electron transfer rate constants at high temperatures in nonpolar and weakly polar solvents. The resulting rate constant expression takes the form[9]

$$k_{NA} = \frac{2\pi}{\hbar}|V|^2 \frac{1}{\sqrt{4\lambda_o \pi k_B T}} \sum_{n=0}^{\infty} \exp(-S)\left(\frac{S^n}{n!}\right) \times \exp\left[-\frac{(\Delta_r G + \lambda_o + nh\nu)^2}{4\lambda_0 k_B T}\right] \quad (1)$$

where λ_o is the medium reorganization energy, $\Delta_r G$ is the Gibbs energy change between the locally excited (LE) state and the charge-separated (CS) state, and $S = \lambda_v/(h\nu)$ where λ_v is the internal reorganization energy. The $h\nu$ term is the energy spacing of the single effective quantum mode that is coupled to the electron transfer reaction. These last two terms account for the high frequency component of the reorganization energy, and for these systems it is characteristic of the donor and acceptor groups. See ref 8 for a more detailed description.

Previously, $\Delta_r G$(LE → CS) for **1**, **2**, and **3** was determined experimentally from the kinetic data in the solvents toluene, mesitylene, and *p*-xylene.[10,11] In these systems, an equilibrium exists between the charge-separated state and the locally excited state so that $\Delta_r G$ could be determined experimentally. These data were used to calibrate the solute-molecule parameters of a molecular solvation model. [12−14]

This study extends the earlier work by exploring how the solvent dynamics affects the charge transfer of **1**, **2**, and **3** in *N*-methylpropionamide (NMP). These solute molecules are chosen to explore how the change from a nonadiabatic electron transfer mechanism to a solvent-controlled electron transfer mechanism depends on the strength of the solute molecule's electronic coupling. NMP was chosen as a solvent because it has a large static dielectric constant and slow polarization response (Table 1), which results from its hydrogen bonded structure, in the hope that these features would make the dynamical solvent effect more strongly manifest. The solvation response of the solvent was quantified by the dynamic Stokes shift of dye molecule fluorescence; as reported earlier, we use the correlation time for the solvation response rather than attempt to include its nonexponentiality explicitly.[5] The Zusman model was used to fit the experimental results over a wide temperature range (from 337 to 230 K) and obtain an outer-sphere solvent

[†] University of Pittsburgh.
[‡] University of New South Wales.

10.1021/jp807412c CCC: $40.75
Published on Web 01/15/2009

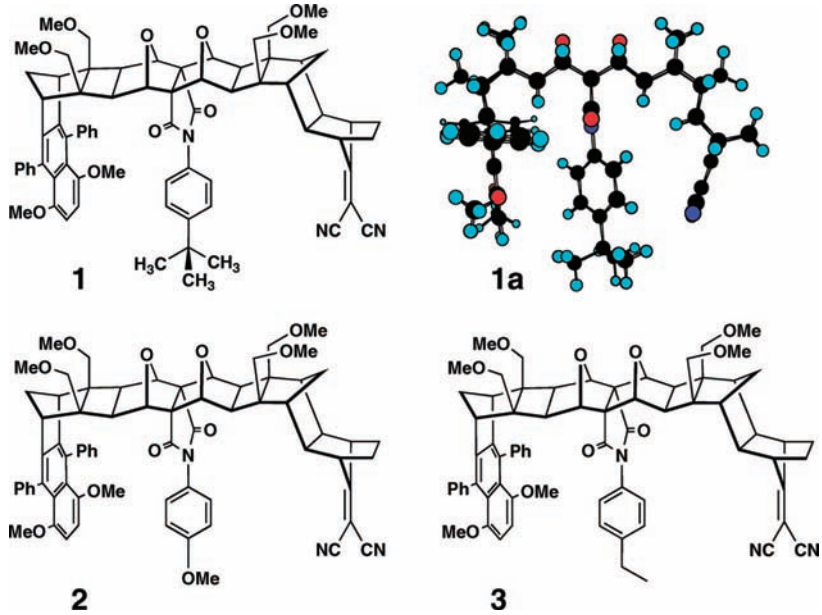

Figure 1. The U-shaped donor-bridge-acceptor (DBA) molecules, **1**, **2** and **3**, having different pendant units (*t*-butylphenyl for **1**, methoxyphenyl for **2**, and ethylphenyl for **3**). The profile of the B3LYP/6-31G(d) optimized geometry of **1** is shown in 1a and illustrates the relative dispositions of the two chromophores and the pendant group.

TABLE 1: Properties of Solvent NMP at 303 K

solvent	n^a	$\epsilon_S{}^a$	τ_D (ps)^b	τ_S (ps)^c	η (cP)^a	μ (D)^d
NMP	1.43	164.4	100	42	4.60	4.29

[a] The refractive index n, relative static dielectric constant ϵ, and shear viscosity η are taken from the Beilstein database. [b] Taken from ref 5. [c] The solvation time is extracted from the best fit of the dynamic Stokes shift measurements, ref 5. [d] The dipole moment μ was calculated using Gaussian/MP2/6-31G.

TABLE 2: Fitting Parameters for 1, 2, and 3 in NMP at 295 K[a]

compound	$^b\|V\|$ (cm^{-1})	$\lambda_0{}^b$ (eV)	Δ_rG^b (eV)
1	90	1.24	−0.35
2	273	1.59	−0.57
3	147	1.50	−0.52

[a] Values of $\lambda_V = 0.63$ eV and $\hbar\omega = 1600$ cm^{-1} are determined from charge-transfer spectra of related species. [b] Obtained from the fit keeping the electronic coupling $|V|$ the same as obtained from previous study for **2** and **3** but modifying the value for **1**.

reorganization energy (λ_0) and Δ_rG for **1**, **2**, and **3** in NMP (Table 2). The experimental rates in the low-temperature regime are analyzed and discussed in terms of three different models that account for solvent dynamics.

II. Background

Electron transfer reactions are commonly viewed as occurring in one of three possible regimes that are distinguished by the strength of their electronic coupling $|V|$ and the characteristic response time of the solvent medium. When the electronic coupling is weak $|V| \ll k_BT$ and the solvation response is rapid, the reaction is nonadiabatic (dashed curve in Figure 2) and the rate constant is proportional to $|V|^2$. In this regime, the system may move through the curve-crossing region $q^{\pm}$ many times before the electronic state change occurs; hence the electronic tunneling event (curve hopping) is the rate-limiting step. A second regime is adiabatic electron transfer, where $|V| \gg k_BT$ (solid curves in Figure 2). In this limit, the electronic state evolves from reactant to product as the nuclear motion proceeds

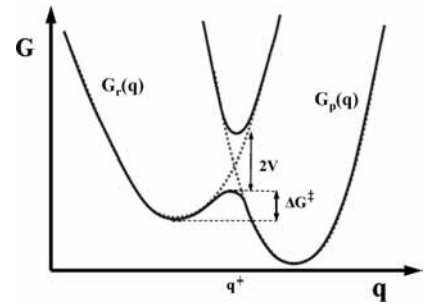

Figure 2. Diagrammatic illustration of the adiabatic (solid curves) − strong coupling − and nonadiabatic (diabatic dashed curves) − weak coupling limits. (Taken from ref 8. Also see ref 15.)

through the transition state. The third regime is solvent-controlled electron transfer, in which the electronic coupling may be weak at the transition state but the characteristic time spent in the curve-crossing region is long enough that nearly every passage through the crossing region results in a change of electronic state. Hence, the reaction appears adiabatic, in the sense that the rate is limited by the nuclear dynamics rather than by the electron tunneling probability. This latter limit is discussed more in the next sections, in terms of different theoretical models.

A. Zusman Model. According to Zusman,[16−18] the electron transfer rate constant (k_{ET}) can be expressed as a serial combination of the normal nonadiabatic electron transfer rate constant (k_{NA}) and a solvent-controlled electron transfer rate constant (k_{SC}), namely

$$\frac{1}{k_{ET}} = \frac{1}{k_{SC}} + \frac{1}{k_{NA}} \tag{2}$$

When $k_{SC} \gg k_{NA}$, the overall electron transfer rate k_{ET} can be described well by the semiclassical expression for k_{NA} (eq 1). On the other hand, if the solvent's polarization relaxation is the rate-limiting step then $k_{ET} \sim k_{SC}$ because $k_{SC} \ll k_{NA}$, and the contribution of k_{NA} to the overall rate constant is small.

In the classical limit (quantized vibrational modes ignored), Zusman finds that k_{SC} can be expressed by

$$k_{SC,Z} = \frac{1}{\tau_S}\sqrt{\frac{\lambda_0}{\pi^3 k_B T}}\sin\left[\pi\sqrt{\frac{\Delta G^{\ddagger}}{\lambda_0}}\right]\exp(-\Delta G^{\ddagger}/k_B T) \quad (3)$$

in which $\Delta G^{\ddagger} = (\Delta_r G + \lambda_0)/(4\lambda_0)$, which predicts that the electron-transfer rate constant is inversely proportional to the solvation time τ_S. Because the solvation time increases rapidly with decreasing temperature in viscous solvents, the solvation dynamics can become rate limiting at low temperature. Correspondingly, the solvation time gets faster at higher temperature and the electron transfer rate becomes less dependent on solvent friction as the temperature increases. If we define a reduced electron transfer time τ^*_{ET} by

$$\tau^*_{ET} = \sqrt{\frac{1}{\lambda_0 k_B T}}\frac{\exp(-\Delta G^{\ddagger}/k_B T)}{k_{ET}} \quad (4)$$

and substitute into eqs 2 and 3, we find that

$$\tau^*_{ET,Z} = \frac{\sqrt{\pi^3}}{\lambda_0 \sin\left(\pi\sqrt{\frac{\Delta G^{\ddagger}}{\lambda_0}}\right)}\tau_S + \sqrt{\frac{1}{\lambda_0 k_B T}}\frac{\exp(-\Delta G^{\ddagger}/k_B T)}{k_{NA}} \quad (5)$$

In the approximation that the first term in the summation over vibronic states in eq 1 dominates the sum, the rate constant expression k_{NA} reduces to the classical expression with an effective electronic coupling $|V_{eff}| = |V| \exp(-S/2)$ and eq 5 takes the form.

$$\tau^*_{ET,Z} = \frac{\sqrt{\pi^3}}{\lambda_0 \sin\left(\pi\sqrt{\frac{\Delta G^{\ddagger}}{\lambda_0}}\right)}\tau_s + \frac{\hbar}{\sqrt{\pi}|V_{eff}|^2} \quad (6)$$

Although λ_0 and$\Delta_r G$ are each temperature dependent, their net contribution to the temperature dependence in eq 6 is weak over the temperature range studied so that τ^*_{ET} is effectively a linear function of τ_s.

B. Sparpaglione−Mukamel Model. Sparpaglione and Mukamel have developed a model[19,20] for electron transfer rates in polar solvents that includes dynamical solvent effects and interpolates between the nonadiabatic and adiabatic limits. This model uses a time-correlation function to describe the solvent response, which allows the treatment of non-Debye solvent models. Their expression for the electron transfer rate constant is given by

$$k_{ET,SM} = \frac{2\pi}{\hbar}|V|^2\frac{1}{\sqrt{4\pi\lambda_0 kT} + \frac{2\pi|V|^2\tau_a}{\hbar}}\exp\left(-\frac{(\Delta_r G + \lambda_0)}{4kT\lambda_0}\right) \quad (7)$$

in which the symbols have their usual meaning and τ_a is a characteristic solvent response time. This formulation corresponds to a limit in which the characteristic time $\tau \sim \sqrt{(h^2/8kT\lambda_0)^{1/2}}$ is shorter than solvent timescales relevant to the electron transfer and the back electron transfer is neglected.[21,22] For τ_a short enough, the nonadiabatic limit (classical version of eq 1) is recovered, and in the solvent-controlled limit (τ_a long enough) one finds that

$$k_{SC,SM} = \frac{1}{\tau_a}\exp\left(-\frac{(\Delta_r G + \lambda_0)}{4kT\lambda_0}\right) \quad (8)$$

This latter result differs from Zusman's result (cf. eq 3).

Using the definition of τ^*_{ET} (eq 4) and substituting in equation 9, we find that

$$\tau_{ET,SM} = \frac{\hbar}{\sqrt{\pi}|V|^2} + \frac{\tau_a}{\sqrt{\lambda_0 kT}} \quad (9)$$

Under the approximation that the solvation time is a property of the solvent and not dependent on the details of the solute (e.g., size of dipole moment, radius of the solute), we can use the solvation time from dynamic Stokes Shift measurements[5] to write $\tau_a = \tau_s$. This result differs from that found from the Zusman model. Although a plot of τ^*_{ET} versus τ_s has the same intercept in these models, the slope of the line is predicted to be different.

C. 2D Electron Transfer Model. Sumi, Nadler, and Marcus[23,24] introduced a two-dimensional (2D) electron transfer model to describe the influence of solvent dynamics. This model views the reaction as proceeding along a 2D reaction coordinate, containing a nuclear coordinate (q) and a solvent polarization coordinate (X). They found the reaction rate by solving a diffusion-reaction equation for diffusive motion along X and treating the motion along q through a rate constant $k(X)$, which is X dependent but depends on the fast motions in the normal way (eq 1). The population probability is described by

$$\frac{\partial P(X,t)}{\partial t} = D\frac{\partial}{\partial X}\left[\frac{\partial}{\partial X} + \frac{1}{k_B T}\frac{dV}{dX}\right]P(X,t) - k(X)P(X,t) \quad (10)$$

where D is the diffusion coefficient, $V(X)$ is the effective potential for the solvent polarization coordinate, and $P(X,t)$ is a probability distribution function for the reactant population. This model predicts that solvents with long polarization relaxation times have a *power-law* dependence of the average survival time on the solvent relaxation time. They solve the diffusion reaction equation for four limiting cases. The first case is called the slow reaction limit and corresponds to the motion along X, which is fast compared to the motion along q, so the reaction does not depend on solvent frictional coupling. The second case is known as wide reaction window and represents a situation in which the internal reorganization energy is much larger than the solvent reorganization so that the reaction may proceed at a range of X values but the reaction rates at different X values are the same. In the third (narrow reaction window) and fourth (non-diffusing limit) cases, the motion along the polarization coordinate is slow compared to $k(X)$, and the solvent friction has a significant effect on the electron transfer rate. In the narrow reaction window limit, Sumi and Marcus[23] assume the electron transfer occurs at a particular value of $X = X_0$, and the reaction rate is controlled by the time evolution of the reactant population along X, which can be nonexponential. In the non-diffusing limit, the reaction occurs at a range of X values, and the nonexponentiality of the rate arises from a distribution of $k(X)$.

Although Sumi, Marcus, and Nadler discussed four limiting cases, only two of these are relevant to the present study. One is the slow reaction limit, which applies for the high temperature data reported here, and the other is the narrow reaction window and it applies to the low-temperature data. For the narrow reaction window case, they showed that the average survival time increases gradually with increasing solvent relaxation time with a slope between zero and unity. Also, they found that the logarithm of the average survival time τ_c increases linearly with an increase in the activation barrier and has a slope between zero and one. Hence, the dependence of the average survival time on activation energy barrier$\Delta G^{\ddagger}/(k_B T)$ over some interme-

diate values of activation barrier can be approximated as $\tau_c \propto \exp(\alpha\Delta G^{\ddagger}/(k_B T))$, where α is a parameter between zero and one. Comparison of the experimental data for **1**, **2**, and **3** with this model are discussed in the results section.

III. Experimental Section

The synthesis of the U-shaped supermolecules **1**, **2**, and **3** has been fully described in the Supporting Information associated with refs 10 and 11.

The solvent NMP was purchased from TCI America. NMP was fractionally distilled three times under vacuum. The freshly purified fraction was used in all the experiments. Each solution was freeze−pump−thawed a minimum of seven cycles or more to eliminate dissolved oxygen.

Time resolved fluorescence kinetics of **1**, **2** and **3** were measured using the time-correlated single photon counting technique. Each sample was excited at 330 nm by the frequency-doubled cavity-dumped output of a Coherent CR599−01 dye laser, using DCM (4-dicyanomethylene-2-methyl-6-p-dimethylamino-styryl-4H-Pyran) dye, which was pumped by a mode locked Vanguard 2000-HM532 Nd:YAG laser purchased from Spectra-Physics. The dye laser pulse train had a repetition rate of 300 kHz. Pulse energies were kept below 1 nJ, and the count rates were kept below 3 kHz to prevent pile up effects. All fluorescence measurements were made at the magic angle, and data were collected until a standard maximum count of 10 000 was observed at the peak channel.

The steady-state and time-resolved fluorescence kinetics for **1**, **2**, and **3**, and their donor only analogues were carried out in NMP as a function of temperature (O.D. $\sim$ 0.10). The temperature ranged from 226 K to a high of 353 K. The experimental high range of temperature was controlled by an ENDOCAL RTE-4 chiller and the temperature was measured using a type-K thermocouple (Fisher-Scientific), accurate to within 0.1 °C. Measurements in the lower temperature range employed a VPF Cryostat (Janis Research Company, Inc.) and a Model 321 Autotuning Temperature Controller (LakeShore Cryotronics, Inc.) with a silicon diode sensor.

Temperature measurements were improved from the earlier described design by incorporating another type-T thermocouple directly on the surface of the sample cell to monitor the temperature, in addition to the silicon sensor used for temperature control, which is not directly in contact with the sample cuvette. The temperatures measured at the sample cell's surface are close to those measured when a thermocouple is directly inserted into the liquid sample, within 1 K, but they are systematically higher than the temperature measured from the diode sensor. The worst case was observed at the lowest temperature (220 K), which had a 10 K difference.

The instrument response function was measured using a sample of colloidal $BaSO_4$. The fluorescence decay curve was fit by a convolution and compare method using *IBH-DAS6* analysis software. Independent experiments on individual donor only molecules at the measured temperatures, always a single exponential fluorescence decay, was used to determine the intrinsic fluorescence decay rate of the locally excited state. The DBA molecules, **1**, **2**, and **3**, have a small amount of donor only impurity. The measurement of the donor only molecule's fluorescence decay characteristic for each solvent and temperature allowed this contribution to the decay to be subtracted from the data and obtain the decay law of the DBA molecules.

Fitting the rate constant data by the semiclassical equation (eq 1) and the low-temperature analysis were performed using *Microsoft Excel 2003*. In fits by a molecular solvation model, the electronic coupling was treated as an adjustable parameter for each solute molecule, and the reorganization energy was treated as an adjustable parameter. The internal reorganization parameters were obtained from the charge transfer spectra of a similar compound and were kept fixed because the solute has the same donor and acceptor group. The molecular solvation model was calibrated for **1**, **2**, and **3** in weakly polar and nonpolar solvents, and it was used to predict the Gibb's free energy and reorganization energy in the polar solvent NMP.

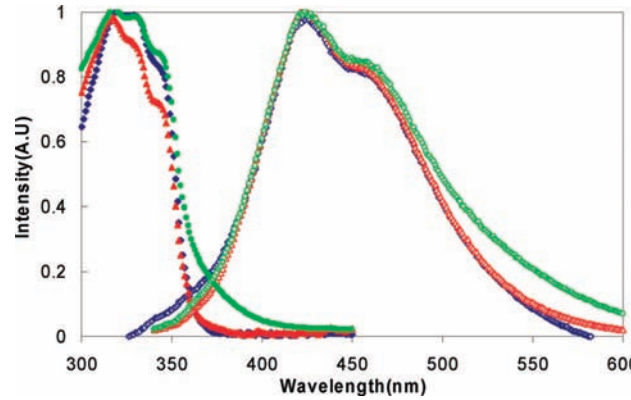

Figure 3. Steady-state absorption and emission spectra of **1** (red), **2** (green), and **3** (blue) in NMP.

IV. Results and Analysis

Steady-State Spectra. Steady-state UV−vis absorption and emission spectra of **1**, **2**, and **3** in NMP are shown in Figure 3. The spectral features of DBA molecules **1**, **2**, and **3** are dominated by the donor 1,4-dimethoxy-5,8-diphenylnaphthalene (DPMN) unit, and excitation at 330 nm produces a locally excited state on the DPMN portion of the molecule. The fluorescence behavior is independent of the excitation energy in this region; the nature of the locally excited state, in terms of the ^1L_a and ^1L_b mixing, is discussed more in refs 10 and 11. **1**, **2**, and **3** differ by the substituent at the para position of the pendant phenyl group, located in the cleft. It is evident that the emission bands of **1** and **3** are nearly identical and that **2** differs somewhat in the red edge/tail. An earlier study in nonpolar and weakly polar solvents showed that a charge transfer band could be identified for **2** in weakly polar and nonpolar solvents. Whereas its emission is expected to be quenched in the highly polar NMP, it may cause some residual broadening on the spectrum's red tail. These results suggest that there is little difference in the steady state emission spectra in these molecules.

Fluorescence Decay Time Analysis. Similar to the results reported earlier for compound **3** in NMP, the fluorescence decays of **1** and **2** in NMP can be fit by a single exponential decay law at high temperature, but become less exponential at lower temperature and are strongly nonexponential at low temperature. In contrast, the decay kinetics of these compounds can be fit by a single exponential decay in acetonitrile at all temperatures studied here, and the nonadiabatic expression (eq 1) provides a good description of the rate constant over the whole temperature range for these compounds. Details can be found in the Supporting Information.

Because the decay law is not single exponential, the electron transfer rate constant is not well-defined in NMP. To quantify the rate in terms of an effective rate constant, a correlation time τ_c is computed from the fluorescence decay law. Because the decay law of the DBA molecule could be described by a sum of exponentials (most commonly two exponentials), τ_c was

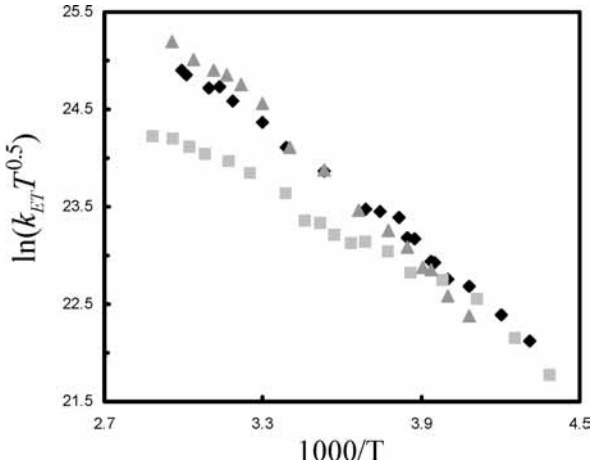

Figure 4. Experimental electron transfer rate constants for **1** (square), **2** (triangle), **3** (diamond) in NMP.

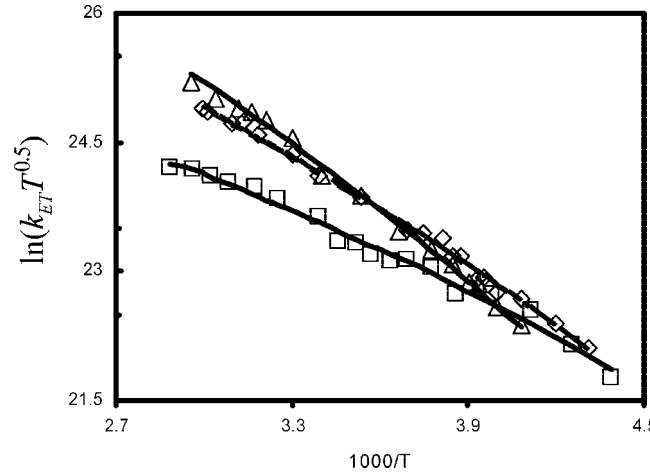

Figure 5. Plots of the electron transfer rate constant data of **1** (square), **2** (triangle), **3** (diamond) in NMP. The straight lines represent the best fit by eq 2.

calculated from, $\tau_c = \sum_i f_i\tau_i$ where, τ_i is the time constant for component i and f_i is the amplitude of component i. As described previously,[4,5] the electron transfer rate is obtained from $k_{ET} = k_{obs} - k_f$, where k_f is the fluorescence decay rate of the donor only molecule and k_{ET} is the experimentally determined electron transfer rate constant. By subtracting the intrinsic lifetime of the locally excited state (modeled as the donor-only lifetime), an effective electron transfer rate constant was found that is $k_{ET} = 1/\tau_c - k_f$.

Figure 4 shows the rate constant data plotted as a function of the inverse temperature. The rate constants for all three compounds are similar at low temperatures; however, they systematically deviate from one another at higher temperatures. The *t*-butyl substituted compound (**1**) deviates most significantly and at a temperature of about 260 to 270 K. The data for **2** and **3** are more similar but show a systematic deviation at temperatures above 310 K. In previous work comparing **3** with a compound containing a propyl pendant group,[5] this overlap of electron transfer rates was explained in terms of a dynamic solvent effect whose importance can be gauged by a characteristic time for the solvent's polarization response. For NMP, a temperature in the 260 to 270 K range corresponds to a solvation time of about 240 ps, and at the relatively higher temperature of 310 K it is about 55 ps. These solvation times are taken from dynamic Stokes shift measurements.[5] This trend in characteristic times for the different solutes correlates with the change in electronic coupling $|V|$ that has been reported for these three molecules, that is, $|V(\mathbf{2})| > |V(\mathbf{3})| > |V(\mathbf{1})|$ and can be predicted by the Zusman and Sparpaglione−Mukamel models, which are discussed later.

Modeling the Rate Constant. Previously, we used a molecular solvation model to fit the high-temperature data in nonpolar and weakly polar solvents and obtained values for the electronic coupling between the donor and acceptor moieties of **1**, **2**, and **3**. We also showed that use of the same model for NMP solvent was unable to fit the data over the whole temperature range. Although eq 1 fits the high-temperature experimental data, it fails to give a good fit in the low-temperature range. This behavior was explained by the importance of the dynamic solvent effect at low temperature. The present analysis uses eq 2 so that the contributions of the dynamic solvent effect are included and a quantitative description of the electron transfer rate constant over the whole temperature range is possible.

Figure 5 shows fits of the experimental rate constant data k_{ET} as a function of temperature to eq 2, using the Zusman model for k_{SC}. In these fits, the reorganization energy and Gibb's energy were treated as adjustable parameters (values are reported in Table 2). Other parameters λ_V, $\hbar\omega$, and τ_s (ref 5) were obtained from previous studies and kept fixed during this analysis. Table 2 lists the Gibb's energy and reorganization energy values obtained from these fits. The electronic coupling values for **2** and **3** were held constant at the values reported previously; however, it was necessary to change the electronic coupling value for **1**, from that reported earlier, to obtain reasonable values of the reorganization energy and Gibb's energy change. To be self-consistent with earlier work, we have taken this new electronic coupling value for **1** and used it to fit our previous data in weakly polar and nonpolar solvents and were able to obtain reasonable fits; this analysis is provided in the Supporting Information. We note that $|V|$ should be considered a dynamical variable whose value fluctuates as the pendant group position changes with respect to the donor and acceptor moieties. The value obtained for $|V|$ by analyzing rate data represents a rms quantity. See ref 8 for more discussion on this point.

From the data at high temperature, it can be observed that the electron transfer rate of **2** is higher than **3** in NMP, and **1** has the lowest electron transfer rate. This trend is consistent with the respective electronic coupling values reported in Table 2. The electronic coupling magnitude of **2** with a methoxy-substituted pendant unit is highest among the three molecules, and can be rationalized in terms of that group's electronic character.[11] The somewhat lower value for the *t*-butyl-substituted pendant, as compared to the ethyl-substituted pendant, could reflect a decrease in overlap that results from steric constraints.

The reorganization energy and Gibb's free energy parameters reported in Table 2 vary somewhat among the three compounds. If one assumes that the first term in the summation of eq 1 dominates over the other terms in its contribution to the sum (and hence to the nonadiabatic rate constant), then the activation barrier for the reaction is $\Delta G^{\ddagger} = (\Delta_r G + \lambda_0)/(4\lambda_0)$. Using the parameters in Table 2, we find that the activation barrier ranges from 0.160 to 0.164 eV for these three compounds. The similarity in the activation barrier (and energetic parameters) is consistent with the similar size, shape, and chemical structure of the molecules. This similarity is found even though the rate constant data appear to deviate substantially from one another as the temperature changes.

The self-consistency of this analysis can be evaluated by considering the dependence of the rate constant on the solvation

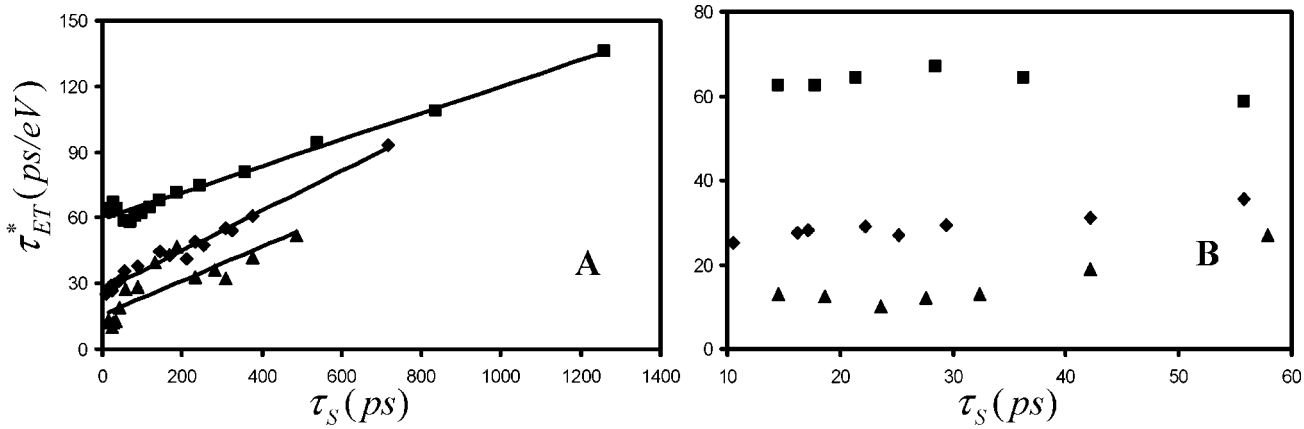

Figure 6. Plot of τ^*_{ET} vs τ_s for **1** (square), **2** (triangle), and **3** (diamond) in NMP. Panel A shows the plot over the whole range of data, and panel B expands the plot in the high temperature region $0 \leq \tau_s \leq 60$ ps (60 ps corresponds to the room temperature) for **1**, **2**, and **3**.

time, via eq 6 or 8. The different kinetic models predict that the electron transfer rate constant is inversely proportional to the solvation time when the reaction proceeds in the solvent friction regime but that it becomes independent of solvent friction when the solvation time is rapid.

Figure 6 plots the value of τ^*_{ET} for **1**, **2**, and **3** in NMP versus the solvation time of NMP over the temperature range of 250 to 350 K. For all of these systems, a good linear correlation between τ^*_{ET} and the solvation time at low temperature is found in the range of large values of τ_s(>60 ps). The intercept from the fit to eq 6 gives an effective electronic coupling $|V_{eff}| = 22$ cm^{-1} for **1**, 49 cm^{-1} for **2**, and 28 cm^{-1} for **3**. Using the fact that $|V| = |V_{eff}| \exp(S/2)$ and $S = 3.2$ (obtained from earlier studies using charge transfer spectra) gives electronic coupling values of 109 cm^{-1} for **1**, 242 cm^{-1} for **2**, and 139 cm^{-1} for **3**. These values are derived by extrapolation from the data in the low-temperature/solvent-controlled limit (eqs 6 and 8); yet they are in excellent agreement with those obtained by analysis over the whole temperature range using eq 2 (compare to values in Table 2) and to values obtained from studies in weakly polar and nonpolar solvents using Matyushov's molecular solvation model (refs 10 and 11).

The dependence of τ^*_{ET} on the solvation time τ_s was fit to eq 6, and the slopes obtained are 0.061 eV^{-1} for **1**, 0.078 eV^{-1} for **2**, and 0.091 eV^{-1} for **3**. In contrast, a calculation of the slopes from the parameters in Table 2 gives 5.20 eV^{-1} for **1**, 4.57 eV^{-1} for **2**, and 5.29 eV^{-1} for **3**. These calculated values are around 50 times bigger than those seen experimentally. Similarly the dependence of τ^*_{ET} on the solvation time, τ_s was fit to eq 9 and the slopes obtained are 0.071 eV^{-1} for **1**, 0.079 eV^{-1} for **2**, and 0.089 eV^{-1} for **3**, which are similar to the slopes obtained from the Zusman model. The slopes obtained theoretically from eq 9 for **1**, **2**, and **3** are 5.63 eV^{-1}, 4.97 eV^{-1}, and 5.12 eV^{-1} respectively, which are also similar to those obtained from eq 6.

Although Zusman and Sparpaglione−Mukamel model comparisons fail to predict the slope quantitatively, they each provide an accurate description of the data otherwise.

Adiabaticity Parameter. Zusman derived a criterion to assess whether the dynamic solvent effect is important in an electron transfer reaction. If the inequality

$$\frac{\pi^2|V|^2\tau_s}{\hbar\lambda_0}\exp(-S) >> \sin\left(\frac{\pi}{2}\left(\frac{\Delta_r G}{\lambda_0}+1\right)\right) \qquad (11)$$

holds, then the solvent friction should be important. If the reaction occurs in the range of a small driving force, $|\Delta_r G| \ll \lambda_0$, and an effective electronic coupling can be defined as $|V_{eff}| = |V| \exp(-S/2)$, then eq 11 becomes $\pi^2\tau_s|V_{eff}|^2/\hbar\lambda_0 \gg 1$. The dynamic solvent effect can be interpreted as a solvent driven change of adiabaticity in the reaction, characterized by an adiabaticity parameter g, where

$$g = \frac{|V_{eff}|^2\pi^2\tau_s}{\hbar\lambda_0} \qquad (12)$$

When $g \gg 1$, the reaction is solvent controlled, and when $g \ll 1$ no dynamic solvent effect is observed. Equation 11 shows that the crossover (g=1) between the nonadiabatic regime ($g < 1$) and the solvent-controlled regime ($g > 1$) depends on τ_S, $|V_{eff}|$, and the solvent reorganization energy.

In the Sparpaglione-Mukamel model one can also define an adiabaticity parameter$g_{SM,}$ which is given by

$$g_{SM} = \frac{|V|^2\tau_S\sqrt{\pi}}{\hbar\sqrt{\lambda_0 k_B T}} \qquad (13)$$

and depends on $|V|$, τ_s, and λ_0; however, it scales as $1/\sqrt{\lambda_0}$ rather than $1/\lambda_0$. When $g_{SM} \ll 1$, eq 12 reduces to the semiclassical eq 1; and when $g_{SM} \gg 1$, the rate constant becomes $k_{ET} = 1/\tau_s\, e^{-\Delta G^{\ddagger}/kT}$ so that the rate is controlled by the solvent relaxation time and the activation energy barrier.

Using the parameters in Table 2 and eq 12, the Zusman model predicts that the dynamic solvent effect should manifest itself when $\tau_s \gg 24$ ps for **1**, $\tau_s \gg 2$ ps for **2**, and $\tau_s \gg 6$ ps for **3** in NMP. The experimental results (Figure 4) indicate that **2** and **3** are in the solvent-controlled limit (coalescence of rates) when τ_s is near 56 ps, which fulfills the Zusman condition. For **1**, the solvent-controlled limit is reached at around 240 ps, again fulfilling the Zusman condition. These comparisons show that the experimentally observed trend in the rate data can be understood via the Zusman model.

The adiabaticity parameter obtained from the Sparpaglione−Mukamel model can be used to draw similar comparisons. In this case, the model predicts that the solvent dynamics are important when $\tau_s \gg 37$ ps for **1**, $\tau_s \gg 5$ ps for **2**, and $\tau_s \gg 12$ ps for **3** in NMP. These values are little different from those obtained using the Zusman model.

Though the Zusman model and Sparpaglione−Mukamel analysis provide very good agreement between the effective electronic coupling values obtained from the low-temperature analysis with those obtained from eq 1 at high temperatures, they overestimate the scaling with the solvent response time (slopes in part A of Figure 6). This failure could result from our modeling of the characteristic polarization relaxation times

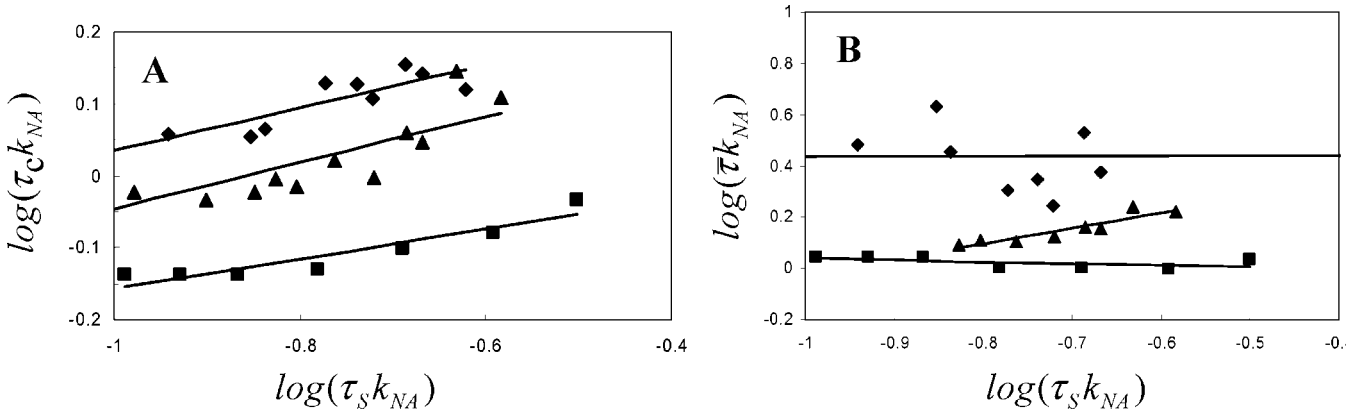

Figure 7. Plot of $\log(\tau_c k_{NA})$ versus $\log(\tau_s k_{NA})$ for **1** (square), **2** (triangle), and **3** (diamond) in NMP (panel A). Plot of $\log(\tau_s k_{NA})$ vs $\log(\tau_s k_{NA})$ for **1** (square), **2** (triangle), and **3** (diamond) in NMP (panel B). These plots show only the low-temperature range. k_{NA} is extracted from the fit of the high temperature data to the nonadiabatic model.

τ_s and τ_a in those models. In both cases, the polarization relaxation times were modeled as the correlation time found from dynamic Stokes shifts measurements of a dye molecule in the solvent NMP. The solvation response in NMP is nonexponential, and it may be that the faster components of the solvation response control the electron transfer dynamics. If so, then the solvation time used here is too large by some factor and this could account for a decreased slope.

2D View of Reaction. In the Sumi−Marcus[23] description, the reaction rate is quantified by considering the average survival probability $Q(t)$ of the locally excited state. $Q(t)$ is the fraction of reactant molecules that have not transferred their electron by time t, and it can be obtained directly from the fluorescence decay law. They considered both the correlation time $\tau_c = \int_0^\infty Q(t)\mathrm{d}t$ and the average decay time $\bar{\tau} = [\int_0^\infty t \cdot Q(t)\,\mathrm{d}t]/\tau_c$ to describe their results. These survival times provide valuable information about the time scale and temporal characteristics of the reaction rate. For example, if $\tau_c = \bar{\tau}$ then $Q(t)$ is a single exponential decay, whereas $\tau_c \neq \bar{\tau}$ indicates a nonexponential decay law. Performing this analysis for the kinetics of **1**, **2**, and **3** in NMP substantiates the inferences drawn above and the manifestation of solvent friction effects.

Figure 7 displays plots of $\log(\tau_c k_{NA})$ (panel A) and $\log(\bar{\tau} k_{NA})$ (panel B) as a function of $\log(\tau_s k_{NA})$ in NMP for **1**, **2**, and **3** over the low-temperature range studied here. k_{NA} is extracted from the fit of the high-temperature kinetic rate data to the nonadiabatic semiclassical electron transfer model. The shift of the solute data from one another may be understood from their different λ_v/λ_0 values as shown by Sumi and Marcus.[23] In our study, because $\lambda_v/\lambda_0 \sim 0.5 < 1$ and $\exp(-\Delta G^{\ddagger}/(k_B T)) < 1$, the reaction proceeds in the narrow reaction window limit. According to Nadler and Marcus,[24] the log−log plots will be linear with a slope of unity in the classical limit ($\lambda_v/\lambda_0 = 0$), but the slope will lie between 0 and 1 for other values of λ_v/λ_0. From part A of Figure 7, it is clear that the product of τ_c and k_{NA} increase gradually as a function of $\tau_s k_{NA}$. The slope for **1** is 0.21, for **2** is 0.32, and for **3** is 0.30, which is less than unity as predicted by Nadler and Marcus.[24] In part B of Figure 7, the data points for **1** and **2** show a somewhat linear behavior, suggesting a dynamic solvent effect, but for **3** the data are too scattered to draw a conclusion.

To better understand the data in terms of the 2D model, Figure 8 shows plots of $\log(\tau_c k_{NA,max})$ as a function of $\Delta G^{\ddagger}/(k_B T)$ for **1**, **2**, and **3** over the whole temperature range. $k_{NA,max}$ stands for the electron transfer rate constant evaluated from the semiclassical nonadiabatic electron transfer rate under zero activation barrier. According to the Sumi-Marcus model,[23] the plot in Figure 8 should be linear, as observed. The data for **1**, **2**, and **3** in Figure 8 have slopes ranging from about 0.45 to 0.52, which are less than unity, as predicted by the model.[24] These experimental findings indicate that the solvent response influences the electron transfer rate constant, and that the effect becomes more pronounced with increasing solvent relaxation time at low temperature.

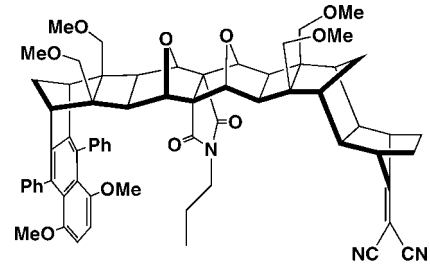

4, $|V| \sim 62\,\mathrm{cm}^{-1}$

Comparing **1**, **2**, and **3** with another previously studied molecule **4** (reported to have $|V| = 62\ \mathrm{cm}^{-1}$) shows a dependence of the observed dynamic solvent effect on the electronic coupling. In each case, the switchover in the mechanism is defined empirically as the temperature at which the rate constant of a solute molecule coincides with that of **2** because it has the highest coupling. With this definition, the switchover for **4** occurs at $\tau_S \sim 309$ ps, for **1** it is reached at around 240 ps, and for **3** it is reached at 56 ps. This comparison shows that as the electronic coupling values decrease (Table 2) a slower (more sluggish) polarization relaxation is required to observe a dynamic solvent effect.

V. Discussion and Conclusions

This work explores the transition from nonadiabatic electron transfer to solvent-controlled electron transfer for the U-shaped DBA molecules **1**, **2**, and **3** in NMP. The rate data were compared with models that interpolate between the nonadiabatic and solvent-controlled limits; each of the models provides a semiquantitatively accurate description of the behavior in terms of a dynamic solvent effect. The solvent-controlled limit is manifest even though the electronic couplings lie in the intermediate ($|V| \sim k_B T$) to weak ($|V| < k_B T$) coupling regime.

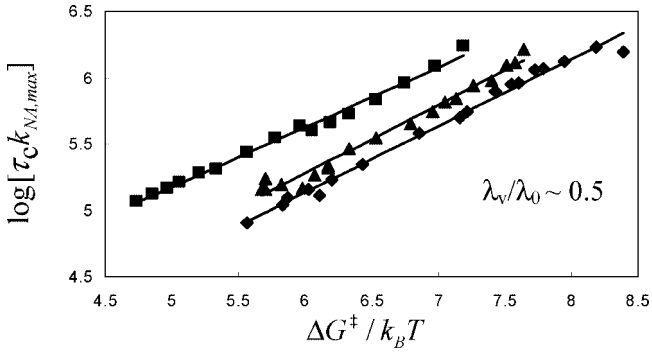

Figure 8. Plot of $\log(\tau_c k_{NA,max})$ versus $\Delta G^{\ddagger}/k_B T$ for **1** (square), **2** (triangle), and **3** (diamond) in NMP (panel B). k_{NA} is extracted from the fit of the high-temperature data to the nonadiabatic model.

The electron transfer rate constants were fit by the Zusman model over the whole temperature range. Fitting the experimental rate data to the model was used to obtain the Gibb's free energy and the reorganization energy for **1**, **2**, and **3** in NMP (Table 2). As reported in the earlier work, the electron transfer rate constants fall below the nonadiabatic electron transfer rates predicted by the semiclassical equation.

The locally excited state's population decay changes from a single exponential decay at high temperature to a nonexponential decay, which can be analyzed in terms of two exponentials at low temperature in these molecules. This observation indicates that the time evolution of the reactant population along X must be considered at low temperature and increasing solvation time This conclusion is supported by the difference between the correlation time and average time (Figure 7) measures of the rate, as anticipated by the Sumi−Marcus model.

The low-temperature rate constants for **1**, **2**, and **3** in NMP were compared to three different models for the solvent dynamical effect. Both Zusman's model[16−18] and Sparpaglione−Mukamel's model[19,20] predict that the rate constant should correlate with the characteristic time for the solvent polarization relaxation. The data were shown to correlate with the characteristic solvation rate, $1/\tau_s$, which was modeled for NMP by dynamic Stokes shifts measurements on a dye molecule. At high temperature, the rate constant is found to be independent of τ_s, and at low temperature the rate constant scales linearly with $1/\tau_s$; see Figure 6. Quantitative comparisons with these models give an electronic coupling that is in good agreement with the value found using the semiclassical electron transfer expression (eq 1) to fit the rate data at high temperatures. In addition, the models' criteria for adiabaticity (g parameter) are satisfied, however the models' estimates of the characteristic time for the transition from nonadiabatic to solvent control (via the criterion of $g = 1$) are somewhat weaker than what is found using the solvation time from the dynamic Stokes shift measurements. Although the plot of τ^*_{ET} versus the solvation time τ_s reveals a linear correlation at low temperatures, the slopes of the plot disagree significantly from the theoretical prediction.

Different possibilities can be identified for the discrepancy between the predictions of Zusman's model and the observed dependence of τ^*_{ET} on τ_s. One possibility is that the solvation time obtained from the dynamic Stokes shift measurement is not the correct measure.[5] The solvation response of NMP was found to be nonexponential, so that a correlation time for the response was calculated and used in the comparisons of Figure 6. It may be that this characteristic time is not appropriate for the electron transfer rate. For example, it may be that only a portion (e.g. the high-frequency/short-time components) of the response function is relevant for the electron transfer reaction. A second limitation of the Zusman and Sparpaglione−Mukamel treatments arises from their high friction (Smoluchowski) limit for the solvent frictional coupling. Recently, Gladkikh[25] et al. extended Zusman's ideas to the intermediate friction regime and different barrier shapes. They found that the Zusman model overestimated the transfer rate by up to 10^3 and that the dynamics is a sensitive function of $|V|$ (or distance). Although quantitative details of these models may be questioned, they appear to capture the physical essence of the process and link with the correct nonadiabatic limit.

The electron transfer in **1**, **2**, and **3** appears to lie in the narrow reaction window limit of the Sumi−Nadler−Marcus treatment. The ratio of $\lambda_v/\lambda_0 \sim 0.5$ and the nonexponentiality of the locally excited state's population decay support the interpretation that the reaction proceeds in the narrow reaction window regime. In this limit, the electron transfer reaction occurs predominantly at a particular solvent polarization value of X_0, and the nonexponentiality arises from the time evolution of the reactant population along X. Other considerations of the Sumi−Marcus treatment, for example the electron transfer rate is proportional to the solvation rate, are similar to the Zusman prediction. The important difference between the two models in this limit is that Sumi−Marcus predicts a nonexponential decay law, as observed, whereas the Zusman and Sparpaglione−Mukamel treatments do not explicitly address this issue. The Sumi−Marcus treatment successfully explains the electron transfer behavior of **1**, **2**, and **3** at low temperature in NMP; however, it is difficult to draw direct quantitative comparisons with the model.

The characteristic solvation time required to observe the solvent dynamic effect increases with decreasing electronic coupling values. This trend can be explained from the Zusman and Sparpaglione−Mukamel models. According to eqs 12 and 13, the τ_s should decrease with increasing electronic coupling $|V|$ to satisfy the criterion $g = 1$.

By exploring the electron transfer dynamics of three different U-shaped molecules as a function of temperature in the slowly relaxing solvent NMP, the change in electron transfer mechanism from a nonadiabatic reaction to a friction controlled reaction is observed. Comparison to different theoretical models indicates that the solvent dynamics plays an important role in the electron transfer. The observation that the decay law becomes nonexponential as the solvent relaxation time slows down supports the conclusion that solvent dynamics affect the electron transfer at lower temperature. This study also provides new insights into the factors governing the dynamics of electron transfer through nonbonded contacts in the solvent-control limit.

Acknowledgment. This work was supported by the US National Science Foundation (CHE-0415457 and CHE-0718755) and by the Australian Research Council. The authors also thank Dr. R. A. Butera for technical assistance.

Supporting Information Available: Fluorescence data and an experimental setup diagram. This material is available free of charge via the Internet at http://pubs.acs.org.

References and Notes

(1) Su, S.-G.; Simon, J. D. *J. Chem. Phys.* **1988**, *89*, 908.
(2) Okada, A. *J. Phys. Chem. A* **2000**, *104*, 7744–7750.
(3) McGuire, M.; McLendon, G. *J. Phys. Chem.* **1986**, *90*, 2549–2551.
(4) Liu, M.; Waldeck, D. H.; Oliver, A. M.; Head, N. J.; Paddon-Row, M. N. *J. Am. Chem. Soc.* **2004**, *126*, 10778–10786.
(5) Liu, M.; Ito, N.; Maroncelli, M.; Waldeck, D. H.; Oliver, A. M.; Paddon- Row, M. N. *J. Am. Chem. Soc.* **2005**, *127*, 17867–17876.

(6) Napper, A. M.; Read, I.; Waldeck, D. H.; Head, N. J.; Oliver, A. M.; Paddon-Row, M. N. *J. Am. Chem. Soc.* **2000**, *122*, 5220–5221.

(7) Napper, A. M.; Head, N. J.; Oliver, A. M.; Shephard, M. J.; Paddon-Row, M. N.; Read, I.; Waldeck, D. H. *J. Am. Chem. Soc.* **2002**, *124*, 10171–10181.

(8) Zimmt, M. B.; Waldeck, D. H. *J. Phys. Chem. A* **2003**, *107*, 3580–3597.

(9) (a) Jortner, J. *J. Chem. Phys.* **1976**, *64*, 4860. (b) Bixon, M.; Jortner, J. *Adv. Chem. Phys.* **1999**, *106*, 35.

(10) Liu, M.; Chakrabarti, S.; Waldeck, D. H.; Oliver, A. M.; Paddon-Row, M. N. *Chem. Phys.* **2006**, *324*, 72.

(11) Chakrabarti, S.; Liu, M.; Waldeck, D. H.; Oliver, A. M.; Paddon-Row, M. N. *J. Am. Chem. Soc.* **2007**, *129*, 3247–3256.

(12) Read, I.; Napper, A.; Zimmt, M. B.; Waldeck, D. H. *J. Phys. Chem. A.* **2000**, *104*, 9385–9394.

(13) Matyushov, D. V.; Voth, G. A. *J. Chem. Phys.* **1999**, *111*, 3630.

(14) Gupta, S.; Matyushov, D. V. *J. Phys. Chem. A* **2004**, *108*, 2087–2096.

(15) Marcus, R. A.; Sutin, N. *Biochim. Biophys. Acta* **1985**, *811*, 265.

(16) Zusman, L. D. *Electrochim. Acta* **1991**, *36*, 395.

(17) Zusman, L. D. *Chem. Phys.* **1980**, *49*, 295.

(18) Zusman, L. *J. Chem. Phys.* **1995**, *102*, 2580.

(19) Sparpaglione, M.; Mukamel, S. *J. Chem. Phys.* **1988**, *88*, 3263.

(20) Sparpaglione, M.; Mukamel, S. *J. Chem. Phys.* **1988**, *88*, 4300.

(21) Ponnu, A.; Sung, J.; Spears, K. G. *J. Phys. Chem. A* **2006**, *110*, 12372–12384.

(22) Moran, A. M.; Aravindan, P.; Spears, K. G. *J. Phys. Chem. A* **2005**, *109*, 1795–1801.

(23) Sumi, H.; Marcus, R. A. *J. Chem. Phys.* **1986**, *84*, 4894.

(24) Nadler, W.; Marcus, R. A. *J. Chem. Phys.* **1987**, *86*, 3906.

(25) Gladkikh, V.; Burshtein, A. I.; Rips, I. *J. Phys. Chem. A* **2005**, *109*, 4983–4988.

JP807412C